

Production of unknown neutron-rich isotopes with $Z = 99\text{--}102$ in multinucleon transfer reactions near the Coulomb barrier

Na Tang,^{1,2} Xin-Rui Zhang,³ Jing-Jing Li,² Pei-Wei Wen ,⁴ and Feng-Shou Zhang ^{1,2,5,*}

¹The Key Laboratory of Beam Technology of Ministry of Education, College of Nuclear Science and Technology, Beijing Normal University, Beijing 100875, China

²Institute of Radiation Technology, Beijing Academy of Science and Technology, Beijing 100875, China

³Department of Physics, Guangxi Normal University, Guilin 541004, China

⁴China Institute of Atomic Energy, Beijing 102413, China

⁵Center of Theoretical Nuclear Physics, National Laboratory of Heavy Ion Accelerator of Lanzhou, Lanzhou 730000, China



(Received 27 March 2022; accepted 31 August 2022; published 7 September 2022)

Multinucleon transfer reactions provide a possible access to the synthesis of new neutron-rich isotopes. Within the theoretical framework of a hybrid model combining the dinuclear system model and the GRAZING model together, the transfer reaction is investigated in $^{86}\text{Kr} + ^{248}\text{Cm}$. In this work, it is found that the hybrid model can reproduce experimental transfer cross sections well. After the verification of the hybrid model, the transfer reactions $^{112,124,132}\text{Sn} + ^{249}\text{Cf}$ are investigated by the influence of charge equilibration on the production cross sections of the exotic nuclei. The neutron-deficient projectile ^{112}Sn shows advantages of producing neutron-deficient nuclei, while $^{124,132}\text{Sn}$ are favorable to produce neutron-rich nuclei. In order to obtain available production cross sections of the unknown neutron-rich isotopes with $Z = 99\text{--}102$, the dependence of cross sections on incident energy in the reaction $^{132}\text{Sn} + ^{249}\text{Cf}$ is also investigated. It is found that the reaction $^{132}\text{Sn} + ^{249}\text{Cf}$ at 510 MeV is a potential candidate to produce unknown neutron-rich isotopes of trans-target.

DOI: [10.1103/PhysRevC.106.034601](https://doi.org/10.1103/PhysRevC.106.034601)

I. INTRODUCTION

Up to now, the landscape of nuclear charts has been extended to the $Z = 118$ element that was first discovered by Oganessian and his coauthors through the hot-fusion reaction $^{249}\text{Cf}(^{48}\text{Ca}, 4n)^{294}\text{Og}$ in 2006 [1]. The knowledge of new neutron-rich nuclei located at the southeast of the stability line challenges the experimental and theoretical studies. This is mainly due to the poorly known information about this unexplored area of neutron-rich isotopes of heavy and superheavy elements and the limitations of the existing reaction mechanisms.

The synthesis of neutron-rich nuclei has significant importance not only in nuclear physics (e.g., nuclear models and the evolution of nuclear structures) but also in astrophysics for stellar nucleosynthesis [2,3]. The multinucleon-transfer (MNT) process provides an alternative approach to produce new heavy and superheavy nuclei [4–11]. Watanabe *et al.* demonstrated that MNT reactions become superior to projectile fragmentation reactions around the $N = 126$ shell closure in the $^{136}\text{Xe} + ^{198}\text{Pt}$ reaction [12,13]. Meanwhile many theoretical studies have been performed along $N = 126$ isotones [14–17]. These studies have found that the production cross sections are determined by various possible mechanisms, such as the influence of incident energies [18], shell effects

[19,20], charge equilibrium [21,22] and mass asymmetry effects [23,24], etc.

In the past decades, many actinide nuclei as targets have been employed to produce the unknown neutron-rich isotopes in heavy and superheavy regions [25–28]. The MNT reactions, such as $^{40,48}\text{Ca}$ [29,30], ^{86}Kr , $^{136}\text{Xe} + ^{248}\text{Cm}$ [23], and $^{136}\text{Xe} + ^{238}\text{U}$ [31], were performed in laboratories. Much concerning information has been extracted in the dynamical collision process. It was noted that the cross sections of trans-target elements decreased strongly with the increasing charge number in surviving heavy nuclei. However, in the transfer reaction system $^{238}\text{U} + ^{248}\text{Cm}$, several isotopes of Fm and Md have been synthesized and the cross section has been located at the level of $0.1 \mu\text{b}$ [32–35]. Besides, a target of mixed californium (51% ^{249}Cf , 13% ^{250}Cf , and 36% ^{251}Cf) obtained from decayed ^{252}Cf sources was produced in Dubna [36,37]. This indicated that MNT reactions using ^{249}Cf as a candidate target provide a possible access to obtain and investigate new neutron-rich actinide nuclei.

Plenty of theoretical models are used to describe the MNT reaction, such as the dinuclear system (DNS) model [38–45], the GRAZING model [46–48], the time-dependent Hartree-Fock model [49–52], the Langevin equations [14,53,54], and the improved quantum molecular dynamics model [55–58]. The grazing regime of MNT reactions can be described well by the GRAZING model, such as in $^{136}\text{Xe} + ^{208}\text{Pb}$ [16], $^{136}\text{Xe} + ^{238}\text{U}$ [31], and $^{136}\text{Xe} + ^{248}\text{Cm}$ [48]. However, the collision behaviors cannot be described well with the increasing

*Corresponding author: fszhang@bnu.edu.cn

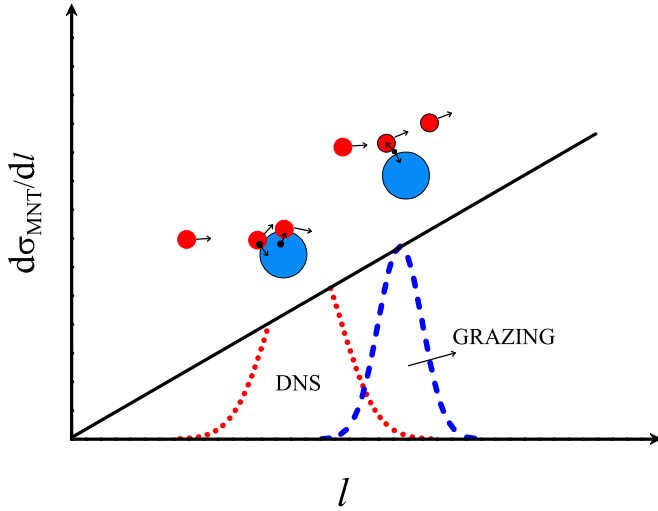


FIG. 1. Diagrammatic map of the distribution of the cross-section differential of MNT responses to GRAZING and DNS models relative to the angular momentum l .

transfer nucleons. By contrast, the DNS model can describe the MNT process in the minor angular momentum regime, where massive nucleon transfer occurs in this region. This model can be used to investigate optimal projectile and target combinations [59] and projectile energies [60]. In Fig. 1, the diagrammatic map described by the DNS model and the GRAZING model of the subdivision of the MNT reactions is shown. The hybrid model (combining the DNS model and the GRAZING model together) allows the results of two models to be taken into account, which is important in explaining the MNT reaction. In Ref. [61], the mechanism of the MNT reaction has been studied by comparing the GRAZING model and the DNS model. The results of these two models are distributed completely in two different areas, which suggests that theoretical results calculated by the hybrid model can reproduce experimental data. Therefore, it is suitable to study the dependence of the actinide yield on the projectile, the target, and the bombardment energy under this hybrid model. We will not only be able to provide the optimal conditions in enhancement of the yield for a given nucleus but also be able to understand possible mechanisms in transfer processes [62].

In this work, the transfer reaction $^{86}\text{Kr} + ^{248}\text{Cm}$ is investigated by the DNS model, the GRAZING model, and the hybrid model, respectively. The transfer reactions $^{112,124,132}\text{Sn} + ^{249}\text{Cf}$ are investigated based on the hybrid model. The influence of charge equilibrium on the production cross sections of exotic nuclei is studied. In order to further predict the production cross sections of the unknown isotopes with $Z = 99-102$, the hybrid model is also investigated in the reaction system $^{132}\text{Sn} + ^{249}\text{Cf}$.

The paper is organized as follows. In Sec. II, we briefly introduce the framework of the DNS model, the GRAZING model and the hybrid model. The results and discussion are presented in Sec. III. A short summary and outlook is given in Sec. IV.

II. THEORETICAL FRAMEWORK

A. DNS model

The evolution of the DNS is a diffusion process in the relative distance between the centers of the interacting nuclei and simultaneously along the mass asymmetry degree. The probability $P(Z_1, N_1, E_1, t)$ of mass distribution for fragments with Z_1 and N_1 can be described by solving the following master equation [22]:

$$\begin{aligned} & \frac{dP(Z_1, N_1, E_1, t)}{dt} \\ &= \sum_{Z'_1} W_{Z_1, N_1; Z'_1, N_1}(t) [d_{Z_1, N_1} P(Z'_1, N_1, E'_1, t) \\ & \quad - d_{Z'_1, N_1} P(Z_1, N_1, E_1, t)] \\ & \quad + \sum_{N'_1} W_{Z_1, N_1; Z_1, N'_1}(t) [d_{Z_1, N_1} P(Z_1, N'_1, E'_1, t) \\ & \quad - d_{Z_1, N'_1} P(Z_1, N_1, E_1, t)], \end{aligned} \quad (1)$$

where $W_{Z_1, N_1; Z'_1, N_1}(t)$ and $W_{Z_1, N_1; Z_1, N'_1}(t)$ are the mean transition probabilities from channel (Z_1, N_1) to (Z'_1, N_1) and (Z_1, N_1) to (Z_1, N'_1) at time t , respectively. d_{Z_1, N_1} denotes the microscopic dimension, namely, the microscopic state number of the fragment for the macroscopic state (Z_1, N_1, E_1) [63]. The local excitation energy E_1 of the composite system is provided by the dissipation of relative kinetic energy. The relation between transition probability and the local excitation energy can be written as

$$\begin{aligned} & W_{Z_1, N_1; Z'_1, N_1}(t) \\ &= \frac{\tau_{\text{mem}} [Z_1, N_1, E_1(Z_1, N_1); Z'_1, N_1, E_1(Z'_1, N_1)]}{d_{Z_1, N_1} d_{Z'_1, N_1} \hbar^2} \\ & \quad \times \sum_{i'i'} |\langle Z'_1, N_1, E_1(Z'_1, N_1), i' | \\ & \quad \times V(t) | Z_1, N_1, E_1(Z_1, N_1), i \rangle|^2. \end{aligned} \quad (2)$$

During the evolution process, one nucleon transfer at each time step is assumed in the DNS model, namely, $Z'_1 = Z_1 \pm 1$ or $N'_1 = N_1 \pm 1$. In Ref. [64], more details are described about memory time τ_{mem} . The local excitation energy of the DNS can be written as

$$\begin{aligned} E_1(Z_1, N_1) &= E_{\text{diss}} - [U(Z_1, N_1, R_{\text{cont}}) \\ & \quad - U(Z_p, N_p, R_{\text{cont}})], \end{aligned} \quad (3)$$

where E_{diss} is the energy dissipated into the composite system, which is related to the incident energy and the entrance angular momentum J . The distribution of the fragments is strongly influenced by the E_{diss} . The potential energy surface (PES) [65,66] plays an important role in the nucleon transfer process, which can be written as

$$\begin{aligned} U(Z_1, N_1, R_{\text{cont}}) &= \Delta(Z_1, N_1) + \Delta(Z_2, N_2) \\ & \quad + V_{\text{cont}}(Z_1, N_1, R_{\text{cont}}). \end{aligned} \quad (4)$$

Here, $\Delta(Z_1, N_1)$ and $\Delta(Z_2, N_2)$ are the mass excesses of the fragments (Z_1, N_1) and (Z_2, N_2) , respectively.

$V_{\text{cont}}(Z_1, N_1, R_{\text{cont}})$ is the effective nucleus-nucleus interaction potential of the two fragments, and R_{cont} is the location of the potential pocket when the nucleus-nucleus potential contains a potential pocket [44]. The position where the nucleon transfer process takes place for the reaction with no potential pockets can be obtained with the equation $R_{\text{cont}} = R_1[1 + \beta_2^{(1)}Y_{20}(\theta_1)] + R_2[1 + \beta_2^{(2)}Y_{20}(\theta_2)] + 0.7$

fm [22]. Here, $R_{1,2} = 1.16A_{1,2}^{1/3}$. $\beta_2^{(i)}$ ($i = 1$ and 2) is the quadrupole deformation parameter of fragment i and can be obtained from Ref. [67].

The following equation gives the production cross section of the primary fragment with proton number Z and neutron number N :

$$\sigma_{\text{pr}}(Z, A, E) = \frac{\pi \hbar^2}{2\mu E_{\text{c.m.}}} \sum_J (2J+1) P_{\text{c}}(E, l) P_{\text{tr}}^{\text{DNS}}(Z, A, E), \quad (5)$$

where $P_{\text{tr}}^{\text{DNS}}(Z, A, E)$ is the production probability of nuclei with charge number Z and mass number A . The sequential statistical evaporation process of excited fragments is calculated with the GEMINI++ code. This code is used to treat not only light particle evaporation and symmetric fission but also all possible binary-decay modes.

B. GRAZING model

The aim of the GRAZING model based on the semiclassical coupled channel equations is to describe the reaction of nucleon-nucleon collisions in the grazing region, particularly the MNT reactions in this region [68]. Therefore, the distance between two colliding heavy nuclei is larger than the sum of their half-density radii. The probability distribution in the excitation energy E^* , the angular momentum M , the transferred neutron number \tilde{N} , and the proton number \tilde{Z} is given by [69]

$$\begin{aligned} P(E_a^*, E_A^*, M_a, M_A, \tilde{N}, \tilde{Z}) &= \langle \tilde{\Psi}(t) | \delta(E_a^* - \hat{H}_a) \delta(E_A^* - \hat{H}_A) \delta(M_a - \hat{M}_a) \delta(M_A - \hat{M}_A) \delta(\tilde{N} - \hat{N}) \delta(\tilde{Z} - \hat{Z}) | \Psi(t) \rangle \\ &= \frac{1}{(2\pi)^6} \int_{-\infty}^{\infty} d\beta_a d\beta_A d\zeta_a d\zeta_A d\gamma_N d\gamma_Z Z(\beta_a, \beta_A, \zeta_a, \zeta_A, \gamma_N, \gamma_Z) \\ &\quad \times \exp[-i\tilde{N}\gamma_N - i\tilde{Z}\gamma_Z - iM_a\zeta_a - iM_A\zeta_A - iE_a^*\beta_a - iE_A^*\beta_A], \end{aligned} \quad (6)$$

where ζ , γ , and β are the Fourier transform parameters for the corresponding excitation energy, nucleon number, and angular momentum. The state vector $|\Psi(t)\rangle$ and its adjoint $\langle \tilde{\Psi}(t)|$ are the solutions of the semiclassical coupled equations in the prior and post representations, respectively, which govern the exchange of nucleons in the mean-field approximation [70]. The characteristic function in the above formula is [71]

$$Z(\beta_a, \beta_A, \zeta_a, \zeta_A, \gamma_N, \gamma_Z) = \langle \tilde{\Psi}(t) | \exp[i\hat{H}_a\beta_a + i\hat{H}_A\beta_A + i\hat{M}_a\zeta_a + i\hat{M}_A\zeta_A + i\hat{N}\gamma_N + i\hat{Z}\gamma_Z] | \Psi(t) \rangle. \quad (7)$$

With the characteristic function, it is able to calculate the correlated probabilities in energy excitation, transfer of nucleons, and angular momentum distribution by integration over it.

The boundary between the grazing inelastic collision and the capture process can be defined by the capture probability P_{c} [47]. Considering the effect of surface deformation, the relative motion of the two colliding nuclei is governed by the classical equation, namely,

$$m_{aA}\ddot{S} = \frac{l^2}{m_{aA}r^3} + \frac{Z_a Z_A e^2}{r^2} - (1 + \kappa) \frac{\partial U_{aA}}{\partial r}, \quad (8)$$

where κ is the factor which determines the changing of force due to the surface collective modes. At the turning point where $\dot{S} < 0$, the capture will happen. When the incident energy is near the Coulomb potential, the quantum penetration effect is considered and P_{c} is expressed as

$$P_{\text{c}}(E, J) = \int P(E_r) T_l(E - E_r) dE_r. \quad (9)$$

Here, $P(E_r)$ is the energy distribution at the distance of closest approach calculated from the characteristic function. $T_l(E)$ is the Wentzel-Kramers-Brillouin penetration formula under the inverse parabolic approximation. The capture probability

can also be obtained in terms of this theory when there is no nominal Coulomb barrier. The influence of inelastic excitation and transfer have been taken into account for the energy distribution $P(E_r)$, this method has been well tested for many fusion reactions in Ref. [71].

Similar to the results obtained by the DNS model, the total production cross sections can be written as a sum over partial waves with the angular momentum J as follows [69]:

$$\begin{aligned} \sigma_{\text{tr}}^{\text{GRAZING}}(Z, A, E) &= \frac{\pi \hbar^2}{2\mu E} \sum_J (2J+1) [1 - P_{\text{c}}(E, J)] \\ &\quad \times P_{\text{tr}}^{\text{GRAZING}}(Z, A, E), \end{aligned} \quad (10)$$

C. The hybrid model

By introducing the DNS model and the GRAZING model, it can be found apparently that the capture probability is key to connect the two models. The capture probability calculated by the GRAZING model is exported and used in the DNS model, which will make the combination more self-consistently. In Fig. 2, the capture probability P_{c} for the reaction system $^{86}\text{Kr} + ^{248}\text{Cm}$ at $E_{\text{c.m.}} = 386$ MeV is plotted as a function of the angular momentum l using the GRAZING model (solid

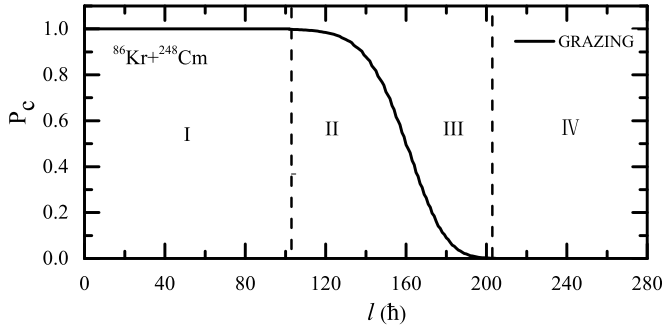


FIG. 2. Capture probability P_c for the reaction system $^{86}\text{Kr} + ^{248}\text{Cm}$ at $E_{c.m.} = 386$ MeV from the GRAZING model (solid line). Areas I and IV correspond to $P_c = 1$ and $P_c = 0$, respectively. $0 < P_c < 1$ locates at areas II and III.

line), which can be divided into four areas of transfer reaction. Massive nucleons are transferred where $P_c = 1$ (I), which can be described by the DNS model. Meanwhile, the GRAZING model does well when few nucleon transfer reactions happen at $P_c = 0$ (IV). At the area of $0 < P_c < 1$, the part of the scattering probability (III) is the domain of the GRAZING model and the capture probability (II) is governed by the DNS model. According to Eqs. (5) and (10), the results of the two models are distributed completely in two different areas. The gradient of the cross section with respect to the angular momentum l for ^{251}Es [panel (a)] and ^{254}Fm [panel (b)] calculated by the GRAZING model (dash-dotted line) and the DNS model (solid line) are shown in Fig. 3, respectively. The similar calculations of other reactions are also investigated in Ref. [61]. The capture probability also varies accordingly

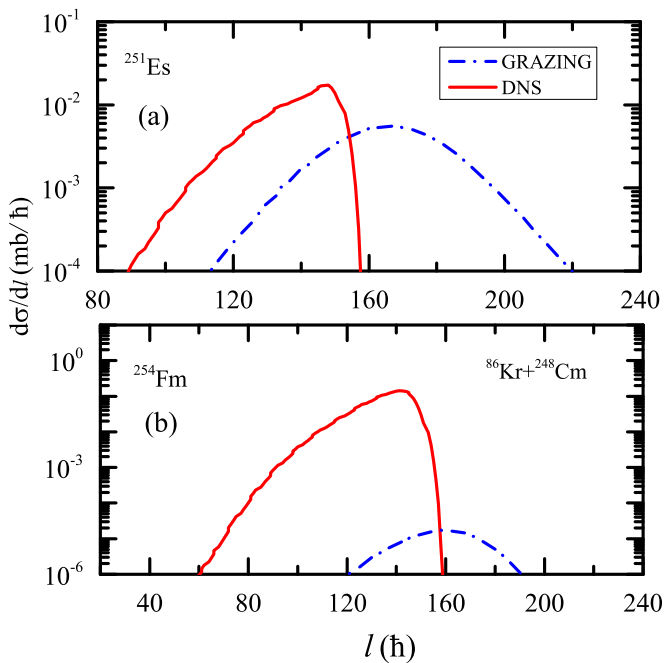


FIG. 3. Gradient of cross section with respect to the angular momentum l for ^{251}Es (a) and ^{254}Fm (b) calculated by the GRAZING model (dash-dotted line) and the DNS model (solid line).

with the angular momentum at different energies. Therefore, the two models can be self-consistently separated using the present method no matter how large the incident energy is. Many experimental data show that the MNT reactions consist of two parts: the direct transfer reaction and the deep inelastic transfer reaction [72,73]. In order to better describe the MNT reactions, the hybrid model combining the DNS model and the GRAZING model together has been proposed. In Ref. [61], more detailed discussions about these models are also given.

As can be seen from Fig. 4, with the purpose to test the reliability of the model, the production cross sections for the isotopes of some targetlike fragments (TLFs) in the reaction system $^{86}\text{Kr} + ^{248}\text{Cm}$ are shown in comparison with the experimental data. The incident energy is $E_{c.m.} = 386$ MeV. The results of the GRAZING model (dashed lines), the DNS model (dash-dotted lines), and the hybrid model (solid lines) are shown for comparison. The experimental data (red solid circles) are taken from Ref. [62]. We can find that the calculated results of the DNS model are in good agreement with the experimental data when more nucleons are transferred. This can be seen obviously from the production cross sections of isotopes in Figs. 4(d)–4(f). Due to the absence of quasielastic scattering in this model, the production cross sections of nuclei near the target are underestimated, such as $^{244-247}\text{Am}$, ^{249}Cm , and $^{245-250}\text{Bk}$, which are 2–3 orders of magnitude lower compared to the experimental data. Careful comparison of the measured cross sections of $^{246,248}\text{Cf}$ with the calculated results reveals that the theoretical values by using the DNS model systematically overestimate the experimental cross sections. However, the error is within 1 to 2 orders of magnitude when comparing the theoretical and experimental values. For Es and Fm, the GRAZING predictions are always larger than the DNS model in the lower-mass regions. The reason is that the grazing angular momentum of the GRAZING model is extracted and used as the boundary for the DNS model, which affects the interaction time calculated with the deflection function method in the DNS model and causes the calculated cross sections to appear narrower. Results of the GRAZING model close to the target nuclei are described well, which is consistent with Ref. [48]. It can be seen clearly that the cross sections of these nuclei are much better when we add up the results of the GRAZING model and the DNS model. Based on the above model test results, we take the hybrid model as the results of our calculations.

III. RESULTS AND DISCUSSION

A. Charge equilibration effect on yields of fragments

MNT reactions have attracted great interest in studying the production cross sections of fragments, especially for bombarding the same target with different projectiles. Furthermore, the hybrid model is extended to investigate MNT reactions. In Fig. 5, the production cross sections of $Z = 97-100$ isotopes are plotted in transfer reactions $^{112,124,132}\text{Sn} + ^{249}\text{Cf}$ at the incident energy $E_{c.m.} = 1.1 \times V_B$. V_B is the Bass barrier in the entrance channel [74]. The corresponding values are 475, 468, and 463 MeV for the reactions

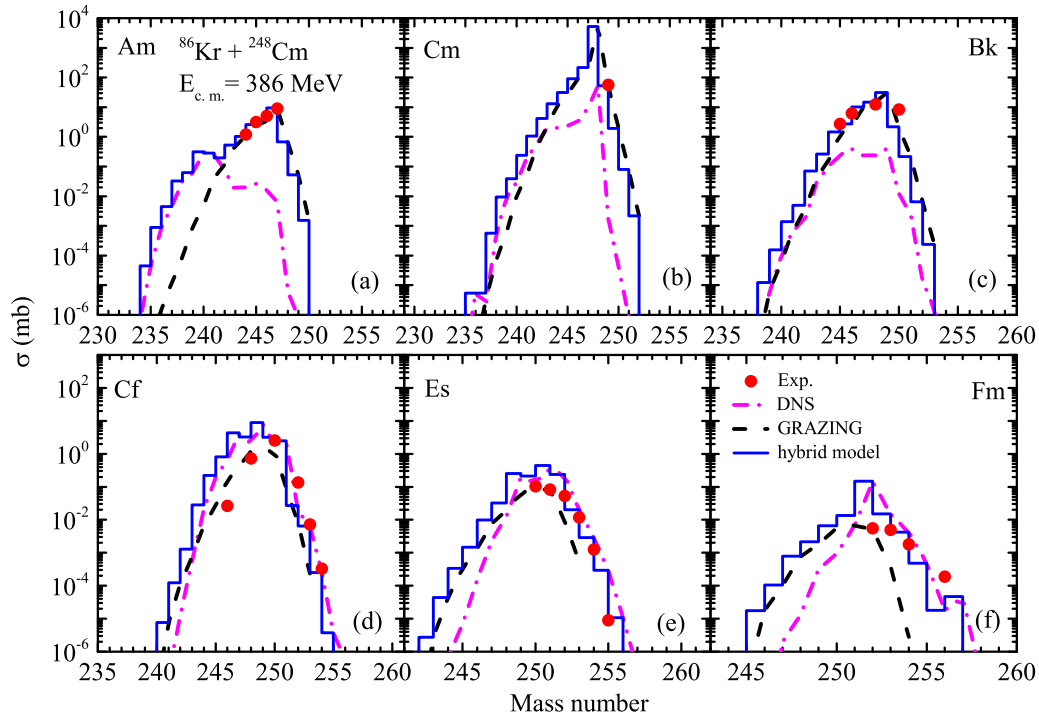


FIG. 4. The isotopic production cross sections of isotopes with $Z = 94$ to $Z = 99$ in the transfer reaction $^{86}\text{Kr} + ^{248}\text{Cm}$. The calculations of the GRAZING model (dashed lines), the DNS model (dash-dotted lines), and the hybrid model (solid lines) are shown for comparison. The incident energy $E_{c.m.} = 386$ MeV. The experimental data (red solid circles) are from Ref. [62]

$^{112}\text{Sn} + ^{249}\text{Cf}$ (dashed lines), $^{124}\text{Sn} + ^{249}\text{Cf}$ (dash-dotted lines), and $^{132}\text{Sn} + ^{249}\text{Cf}$ (solid lines), respectively.

In the two colliding partners of $^{112,124}\text{Sn} + ^{249}\text{Cf}$ reaction systems, the neutron prefers to transfer into the projectile,

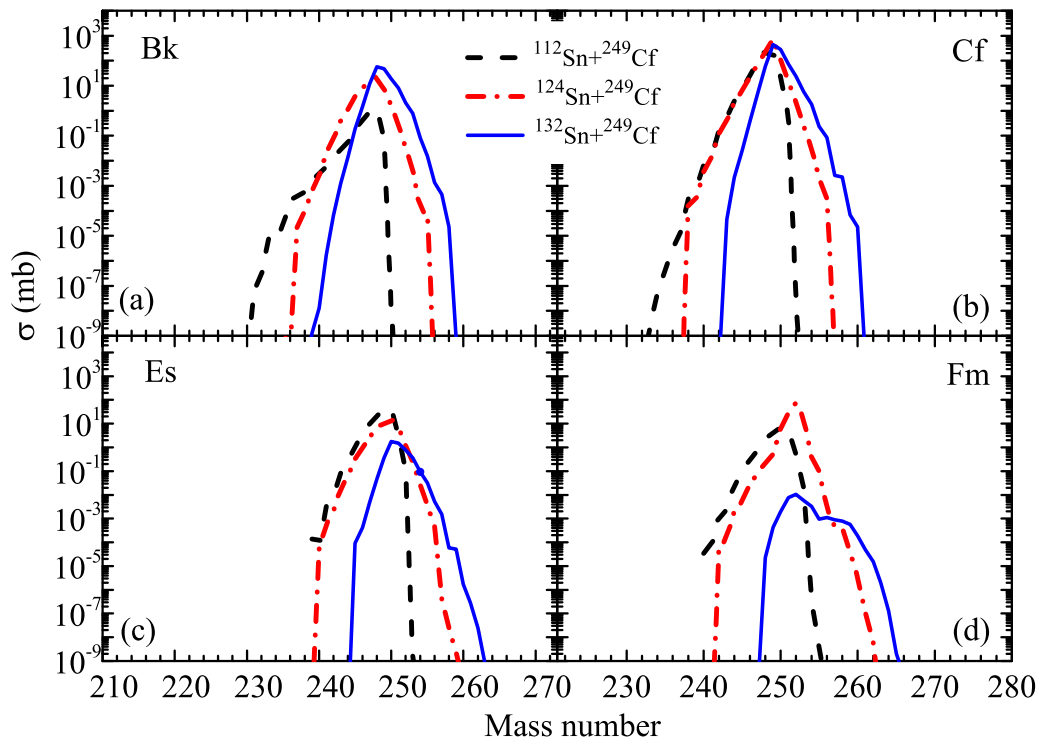


FIG. 5. TLFs' mass distributions from $Z = 97$ to $Z = 100$ in the transfer reactions $^{112}\text{Sn} + ^{249}\text{Cf}$ (black dashed lines), $^{124}\text{Sn} + ^{249}\text{Cf}$ (red dash-dotted lines), and $^{132}\text{Sn} + ^{249}\text{Cf}$ (blue solid lines). The incident energy $E_{c.m.} = 1.10 V_B$.

which is the opposite for the case of proton transfer. It is worth noting that the $^{132}\text{Sn} + ^{249}\text{Cf}$ reaction is more favorable to produce neutron-rich nuclei, with the increasing number of picking up protons, as compared to the $^{124}\text{Sn} + ^{249}\text{Cf}$ reaction. By comparing the obtained results of these reactions, we also find that the reaction with the ^{112}Sn projectile is favorable for productions of neutron-deficient isotopes.

The PES plays an important role in the nucleon transfer process and is strongly influenced by the structural and dynamical properties of the dinuclear system. To clearly describe the injection point of the projectile, the contour plot of the PES of the reaction systems $^{112}\text{Sn} + ^{249}\text{Cf}$, $^{124}\text{Sn} + ^{249}\text{Cf}$, and $^{132}\text{Sn} + ^{249}\text{Cf}$ as functions of N_1 and Z_1 are shown in Figs. 6(a), 6(b), and 6(c), respectively. There is a valley (black line) that can be seen in the two-variable (N_1 , Z_1) driving potential contour plot, and the open circle is the injection point. As can be seen from Fig. 6(a), the injection point of the ^{112}Sn is not in the valley, which is higher than the open circle. With the strong driving force, the nucleon transfer starts from the injection point in the potential energy surface and then continues along the direction with the minimum potential energy of the system. Therefore, the probability distribution starts from the injection point and first preferably reaches the valley. Then, along the valley, it flows simultaneously in the direction of compound nuclear formation and in the direction of symmetry. In Figs. 6(b) and 6(c), for the reactions $^{124}\text{Sn} + ^{249}\text{Cf}$ and $^{132}\text{Sn} + ^{249}\text{Cf}$, the injection points are located at the valley, which coincides with the local minimum of the potential energy surface. The transfer of a nucleon (a proton or a neutron) from the injection point to both sides, in Fig. 6(b) and 6(c), depends on the direction of the lower potential energy surface.

To describe the evolutionary path of the dinuclear system more intuitively, the driving potential of the reactions $^{112,124,132}\text{Sn} + ^{249}\text{Cf}$ is shown in Fig. 6(d), where the subplot is the enlarged view of the injection point of the projectile (open circle). It can be clearly seen that one deep valley appears around the configuration of $^{112}\text{Sn} + ^{249}\text{Cf}$. The configuration of $^{112}\text{Sn} + ^{249}\text{Cf}$ has much higher potential energy compared with that of the other two systems, which means that a nucleon can be transferred after overcoming the higher potential energy. This is because the N/Z ratio of the projection plays an important role in the rearrangement process, which is one of the most important mechanisms to produce neutron-rich nuclei. The N/Z ratios of $^{112,124}\text{Sn}$ are 1.24 and 1.48, which are less than 1.54 ratio of the target ^{249}Cf . In comparison to ^{249}Cf , ^{132}Sn (1.64) with the larger N/Z ratio tends to transfer neutrons to the target. Another reason is that the projectile is a nucleus with a proton shell closure structure at $Z = 50$, and its proton shell usually has a certain stability in the transfer process. At low incident energies, it is more difficult for the target nucleus to transfer protons to the projectile. It can be concluded that the effect of the projectiles on the PES during nucleon transfer is significant with the same target.

To further investigate the process of nucleon transfer, the values of ΔU [$=U(Z_1, N_1, Z_2, N_2) - U(Z_P, N_P, Z_T, N_T)$] and Q_{eg} ($=M_P + M_T - M_{\text{PLF}} - M_{\text{TLF}}$) as functions of the number of transferred neutrons for the reactions $^{112,124,132}\text{Sn} + ^{249}\text{Cf}$

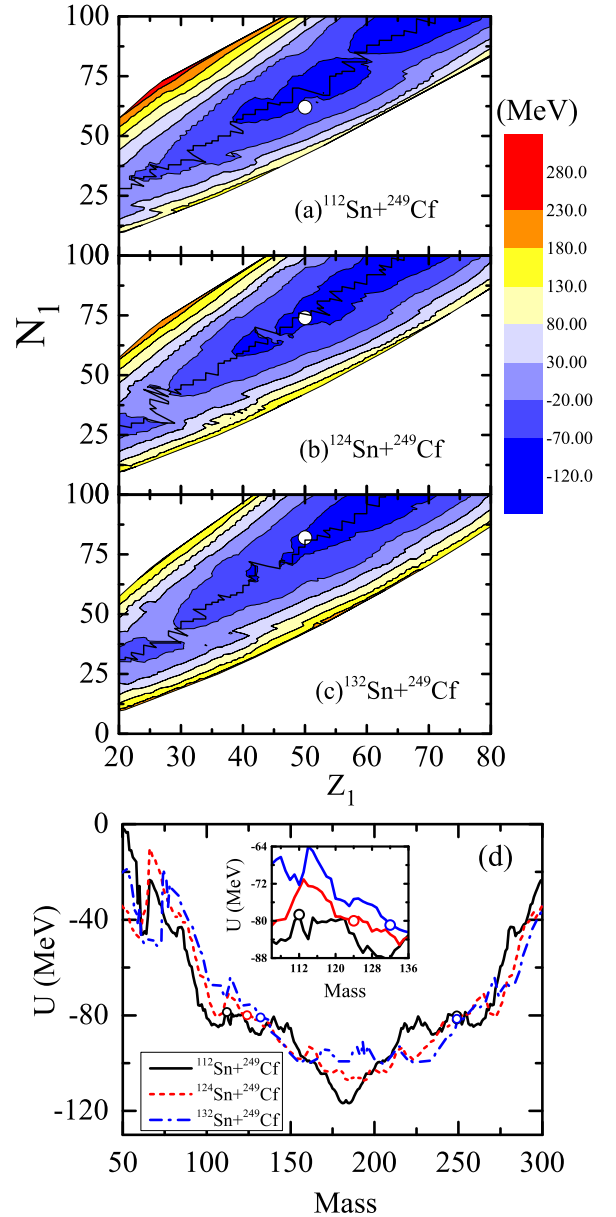


FIG. 6. Contour plot of the driving potential for the reaction systems $^{112,124,132}\text{Sn} + ^{249}\text{Cf}$ as functions of neutron and proton numbers of fragment 1 (a, b, c). The driving potential in the reaction of $^{112,124,132}\text{Sn} + ^{249}\text{Cf}$ (d), where the subplot is the enlarged view of the injection point of the projectile. The incident channels are indicated by open circles.

have been calculated and are shown in Fig. 7. ΔU represents the values of the driving potential needed to be overcome in the nucleon transfer process. It is noticed that the case of the pure neutron stripping channel needs to overcome higher barriers with an increasing number of stripping neutrons, especially in the reaction $^{112}\text{Sn} + ^{249}\text{Cf}$ (the values of ΔU in Fig. 7(a) are 1.04, 6.81, 10.08, and 16.85 MeV, respectively.) Compared to the reactions $^{112,124}\text{Sn} + ^{249}\text{Cf}$ the $^{132}\text{Sn} + ^{249}\text{Cf}$ system with smaller ΔU values tends to transfer neutrons to the target. For instance, when the number of stripping neutrons in the reactions $^{112,124,132}\text{Sn} + ^{249}\text{Cf}$ is four, the values of

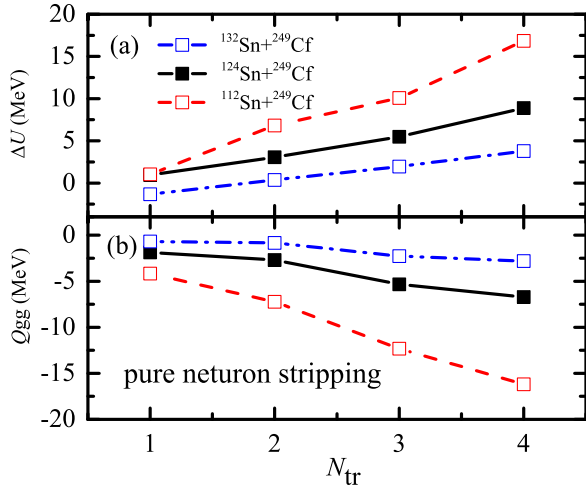


FIG. 7. (a) ΔU [$=U(Z_1, N_1, Z_2, N_2) - U(Z_p, N_p, Z_T, N_T)$] and (b) Q_{gg} ($=M_p + M_T - M_{PLF} - M_{TLF}$) as functions of the neutron stripping number in the reactions $^{112,124,132}\text{Sn} + ^{249}\text{Cf}$.

ΔU are 16.84, 8.89, and 3.79 MeV, respectively. On the other hand, one can see that the values of Q_{gg} of these reactions are all negative in the pure neutron stripping channel. With the increasing number of stripping neutrons from the projectile, the absolute values of Q_{gg} strongly increase. For example, the values of Q_{gg} in the reaction $^{112}\text{Sn} + ^{249}\text{Cf}$ in Fig. 7(b) are -4.16 , -7.23 , -12.33 , and -16.20 MeV, respectively. This means that much energy needs to be absorbed for the ^{112}Sn -induced reaction during the neutron stripping process. With the same target, it can be concluded that the cross sections of transferring neutrons strongly depend on the projectiles in the neutron stripping channel.

B. The incident energies effect on yields of fragments

The effects of charge equilibrium have been understood from what has been discussed above. The $^{132}\text{Sn} + ^{249}\text{Cf}$ reaction is more favorable to produce neutron-rich nuclei. It is instructive to find the optimal incident energy for production cross sections of unknown nuclei. In Fig. 8, we calculate the primary and final cross sections of Md isotopes in the reaction $^{132}\text{Sn} + ^{249}\text{Cf}$ at different incident energies. The dashed lines, solid lines, and dash-dotted lines represent the Md isotopes' production cross sections at $E_{c.m.} = 1.04 V_B$, $E_{c.m.} = 1.10 V_B$, and $E_{c.m.} = 1.20 V_B$, respectively.

The distribution of the primary cross sections of Md shows that the production cross sections of the primary fragments increase overall with the increase of the incident energy. Since the higher incident energy, more nucleons are transformed between projectile and target nuclei. This results in the higher production cross sections of the neutron-rich isotopes. For the isotopic distribution of Md at $E_{c.m.} = 1.10 V_B$ and $E_{c.m.} = 1.20 V_B$, a peak can be found at the left side when the mass number $A = 253$ in Fig. 8. The phenomenon can be explained as the shell effect, which is due to a deformed neutron subshell at $N = 152$ [75]. For the $^{132}\text{Sn} + ^{249}\text{Cf}$ reaction system, the incident energy dependence in the neutron-rich side of the final production cross sections is not sensitive. This is because the higher the incident energy is, the heavier the probability of fission is. This means the survival probability of the primary fragments becomes smaller. It is also clear from the figure that the decay channel of the excited nucleus in this system is mainly a fission process. The final cross sections of Md isotopes are 2–3 orders of magnitude lower than the primary cross sections. Although the final cross sections do not vary much at different incident energies, we find that the cross section at $E_{c.m.} = 1.10 V_B$ is slightly higher than the

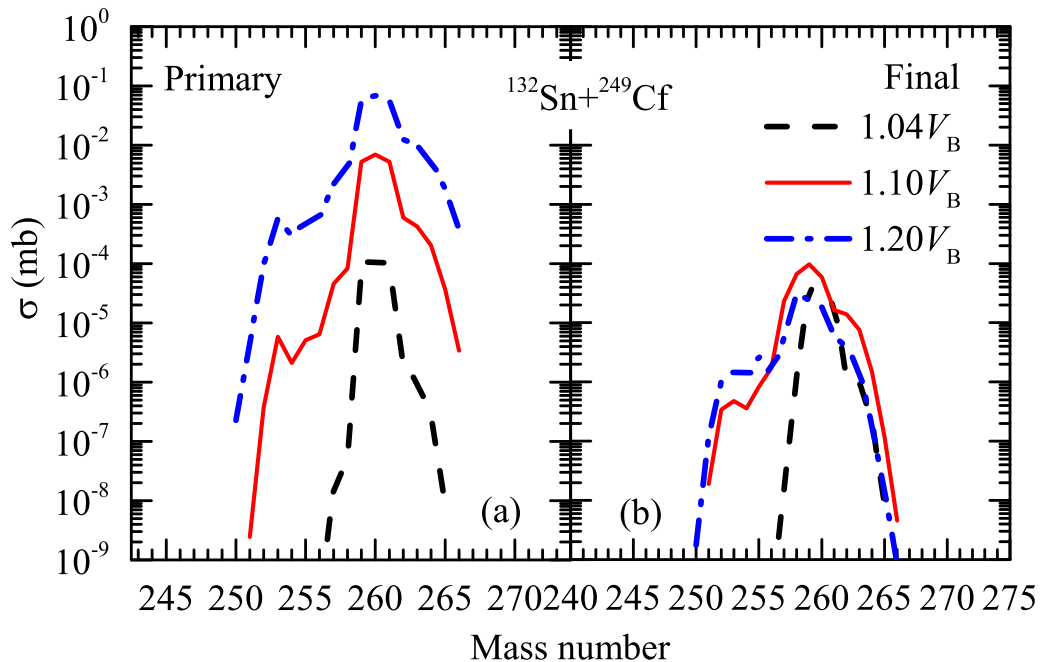


FIG. 8. The primary (a) and final (b) cross sections of Md isotopes in the $^{132}\text{Sn} + ^{249}\text{Cf}$ reaction at different incident energies.

IV. CONCLUSIONS

The DNS model, the GRAZING model, and the hybrid model in the multinucleon transfer process have been tested and compared with the experimental data. It is found that the transfer reaction cross sections can be described well by the hybrid model. The transfer reactions $^{112,124,132}\text{Sn} + ^{249}\text{Cf}$ are investigated. Due to the effect of N/Z ratio equilibration and shell effects, it is hard to transfer protons from ^{249}Cf to the neutron-deficient projectile ^{112}Sn . At the same time, the very neutron-rich nuclei can be produced in the reaction $^{132}\text{Sn} + ^{249}\text{Cf}$. Finally, with the aim of producing trans-target nuclei, we calculated and predicted cross sections of several heavy neutron-rich nuclei in the reaction $^{132}\text{Sn} + ^{249}\text{Cf}$. The predicted production cross sections of the new nuclei $^{258-262}\text{Es}$ are 57.83, 51.34, 1.70, 0.28, and 0.02

nb; of $^{260-264}\text{Fm}$ are 190.71, 48.77, 15.39, 2.00, and 0.13 nb; of $^{261-265}\text{Md}$ are 16.50, 13.82, 7.61, 1.49, and 0.12 nb; and of $^{261,263-267}\text{No}$ are 13.00, 47.19, 29.15, 8.05, 0.88, and 0.08 nb, respectively. It is found that the reaction $^{132}\text{Sn} + ^{249}\text{Cf}$ at 510 MeV is a potential candidate to produce unknown neutron-rich isotopes with $Z = 99-102$.

ACKNOWLEDGMENTS

This work was supported by the National Natural Science Foundation of China under Grants No. 12135004, No. 11635003, No. 11961141004, No. 12105019, and No. 12047513; the Beijing Postdoctoral Research Foundation (Grant No. 2021-zz-089); and the Guangxi Science and Technology Base and Special Talent Program under Grant No. 2021AC19266.

- [1] Y. T. Oganessian, V. K. Utyonkov, Y. V. Lobanov, F. S. Abdullin, A. N. Polyakov, R. N. Sagaidak, I. V. Shirokovsky, Y. S. Tsyganov, A. A. Voinov, G. G. Gulbekian, S. L. Bogomolov, B. N. Gikal, A. N. Mezentsev, S. Iliev, V. G. Subbotin, A. M. Sukhov, K. Subotic, V. I. Zagrebaev, G. K. Vostokin, M. G. Itkis *et al.*, *Phys. Rev. C* **74**, 044602 (2006).
- [2] M. Arnould and S. Goriely, *Prog. Part. Nucl. Phys.* **112**, 103766 (2020).
- [3] K. Langanke and M. Wiescher, *Rep. Prog. Phys.* **64**, 1657 (2001).
- [4] H. Freiesleben and J. Kratz, *Phys. Rep.* **106**, 1 (1984).
- [5] L. Corradi, G. Pollarolo, and S. Szilner, *J. Phys. G: Nucl. Part. Phys.* **36**, 113101 (2009).
- [6] V. V. Desai, W. Loveland, R. Yanez, G. Lane, S. Zhu, A. D. Ayangeakaa, J. P. Greene, F. G. Kondev, R. V. F. Janssens, and P. A. Copp, *Eur. Phys. J. A* **56**, 150 (2020).
- [7] J. Kratz, W. Loveland, and K. Moody, *Nucl. Phys. A* **944**, 117 (2015).
- [8] F. S. Zhang, C. Li, L. Zhu, and P. Wen, *Front. Phys.* **13**, 132113 (2018).
- [9] L. Zhu, C. Li, C. C. Guo, J. Su, P. W. Wen, G. Zhang, and F. S. Zhang, *Int. J. Mod. Phys. E* **29**, 2030004 (2020).
- [10] E. M. Kozulin, V. I. Zagrebaev, G. N. Knyazheva, I. M. Itkis, K. V. Novikov, M. G. Itkis, S. N. Dmitriev, I. M. Harca, A. E. Bondarchenko, A. V. Karpov, V. V. Saiko, and E. Vardaci, *Phys. Rev. C* **96**, 064621 (2017).
- [11] V. V. Desai, A. Pica, W. Loveland, J. S. Barrett, E. A. McCutchan, S. Zhu, A. D. Ayangeakaa, M. P. Carpenter, J. P. Greene, T. Lauritsen, R. V. F. Janssens, B. M. S. Amro, and W. B. Walters, *Phys. Rev. C* **101**, 034612 (2020).
- [12] Y. X. Watanabe, Y. H. Kim, S. C. Jeong, Y. Hirayama, N. Imai, H. Ishiyama, H. S. Jung, H. Miyatake, S. Choi, J. S. Song, E. Clement, G. de France, A. Navin, M. Rejmund, C. Schmitt, G. Pollarolo, L. Corradi, E. Fioretto, D. Montanari, M. Niikura *et al.*, *Phys. Rev. Lett.* **115**, 172503 (2015).
- [13] V. V. Desai, W. Loveland, K. McCaleb, R. Yanez, G. Lane, S. S. Hota, M. W. Reed, H. Watanabe, S. Zhu, K. Auranen, A. D. Ayangeakaa, M. P. Carpenter, J. P. Greene, F. G. Kondev, D. Seweryniak, R. V. F. Janssens, and P. A. Copp, *Phys. Rev. C* **99**, 044604 (2019).
- [14] V. Zagrebaev and W. Greiner, *Phys. Rev. Lett.* **101**, 122701 (2008).
- [15] E. M. Kozulin, E. Vardaci, G. N. Knyazheva, A. A. Bogachev, S. N. Dmitriev, I. M. Itkis, M. G. Itkis, A. G. Knyazev, T. A. Loktev, K. V. Novikov, E. A. Razinkov, O. V. Rudakov, S. V. Smirnov, W. Trzaska, and V. I. Zagrebaev, *Phys. Rev. C* **86**, 044611 (2012).
- [16] J. S. Barrett, W. Loveland, R. Yanez, S. Zhu, A. D. Ayangeakaa, M. P. Carpenter, J. P. Greene, R. V. F. Janssens, T. Lauritsen, E. A. McCutchan, A. A. Sonzogni, C. J. Chiara, J. L. Harker, and W. B. Walters, *Phys. Rev. C* **91**, 064615 (2015).
- [17] Z. Q. Feng, *Phys. Rev. C* **95**, 024615 (2017).
- [18] V. I. Zagrebaev and W. Greiner, *Phys. Rev. C* **87**, 034608 (2013).
- [19] G. G. Adamian, R. V. Jolos, A. K. Nasirov, and A. I. Muminov, *Phys. Rev. C* **53**, 871 (1996).
- [20] E. M. Kozulin, G. N. Knyazheva, S. N. Dmitriev, I. M. Itkis, M. G. Itkis, T. A. Loktev, K. V. Novikov, A. N. Baranov, W. H. Trzaska, E. Vardaci, S. Heinz, O. Beliuskina, and S. V. Khlebnikov, *Phys. Rev. C* **89**, 014614 (2014).
- [21] L. Zhu, J. Su, W. J. Xie, and F. S. Zhang, *Phys. Rev. C* **94**, 054606 (2016).
- [22] L. Zhu, F. S. Zhang, P. W. Wen, J. Su, and W. J. Xie, *Phys. Rev. C* **96**, 024606 (2017).
- [23] K. J. Moody, D. Lee, R. B. Welch, K. E. Gregorich, G. T. Seaborg, R. W. Lougheed, and E. K. Hulet, *Phys. Rev. C* **33**, 1315 (1986).
- [24] I. M. Itkis, E. M. Kozulin, M. G. Itkis, G. N. Knyazheva, A. A. Bogachev, E. V. Chernysheva, L. Krupa, Y. T. Oganessian, V. I. Zagrebaev, A. Y. Rusanov, F. Goennenwein, O. Dorvaux, L. Stuttgé, F. Hanappe, E. Vardaci, and E. de Goés Brennard, *Phys. Rev. C* **83**, 064613 (2011).
- [25] K. D. Hildenbrand, H. Freiesleben, F. Pühlhofer, W. F. W. Schneider, R. Bock, D. V. Harrach, and H. J. Specht, *Phys. Rev. Lett.* **39**, 1065 (1977).
- [26] S. Heinz, H. M. Devaraja, O. Beliuskina, V. Comas, S. Hofmann, C. Hornung, G. Münzenberg, D. Ackermann, M. Gupta, R. A. Henderson, F. P. Heßberger, B. Kindler, B. Lommel, R. Mann, J. Maurer, K. J. Moody, K. Nishio, A. G. Popeko, D. A. Shaughnessy, M. A. Stoyer, and A. V. Yeremin, *Eur. Phys. J. A* **52**, 278 (2016).

- [27] W. Loveland, *Phys. Rev. C* **76**, 014612 (2007).
- [28] T. Welsh, W. Loveland, R. Yanez, J. Barrett, E. McCutchan, A. Sonzogni, T. Johnson, S. Zhu, J. Greene, A. Ayangeakaa, M. Carpenter, T. Lauritsen, J. Harker, W. Walters, B. Amro, and P. Copp, *Phys. Lett. B* **771**, 119 (2017).
- [29] A. Türler, H. R. von Gunten, J. D. Leyba, D. C. Hoffman, D. M. Lee, K. E. Gregorich, D. A. Bennett, R. M. Chasteler, C. M. Gannett, H. L. Hall, R. A. Henderson, and M. J. Nurmia, *Phys. Rev. C* **46**, 1364 (1992).
- [30] S. Heinz, O. Beliuskina, V. Comas, H. M. Devaraja, C. Heinz, S. Hofmann, E. Kozulin, F. Morherr, G. Münzenberg, D. Ackermann, F. P. Heßberger, B. Kindler, B. Lommel, R. Mann, and J. Maurer, *Eur. Phys. J. A* **51**, 140 (2015).
- [31] A. Vogt, B. Birkenbach, P. Reiter, L. Corradi, T. Mijatović, D. Montanari, S. Szilner, D. Bazzacco, M. Bowry, A. Bracco, B. Bruyneel, F. C. L. Crespi, G. de Angelis, P. Désesquelles, J. Eberth, E. Farnea, E. Fioretto, A. Gadea, K. Geibel, A. Gengelbach *et al.*, *Phys. Rev. C* **92**, 024619 (2015).
- [32] M. Schädel, W. Brüchle, H. Gäggeler, J. V. Kratz, K. Sümmerer, G. Wirth, G. Herrmann, R. Stakemann, G. Tittel, N. Trautmann, J. M. Nitschke, E. K. Hulet, R. W. Lougheed, R. L. Hahn, and R. L. Ferguson, *Phys. Rev. Lett.* **48**, 852 (1982).
- [33] W. Loveland, A. M. Vinodkumar, D. Peterson, and J. P. Greene, *Phys. Rev. C* **83**, 044610 (2011).
- [34] J. V. Kratz, M. Schädel, and H. W. Gäggeler, *Phys. Rev. C* **88**, 054615 (2013).
- [35] W. Loveland, *Front. Phys.* **7**, 23 (2019).
- [36] N. T. Brewer, V. K. Utyonkov, K. P. Rykaczewski, Y. T. Oganessian, F. S. Abdullin, R. A. Boll, D. J. Dean, S. N. Dmitriev, J. G. Ezold, L. K. Felker, R. K. Grzywacz, M. G. Itkis, N. D. Kovrizhnykh, D. C. McInturff, K. Miernik, G. D. Owen, A. N. Polyakov, A. G. Popeko, J. B. Roberto, A. V. Sabel'nikov *et al.*, *Phys. Rev. C* **98**, 024317 (2018).
- [37] G. Zhang, C. A. T. Sokhna, Z. Liu, and F.-S. Zhang, *Phys. Rev. C* **100**, 024613 (2019).
- [38] G. G. Adamian, N. V. Antonenko, and A. S. Zubov, *Phys. Rev. C* **71**, 034603 (2005).
- [39] Z. Q. Feng, G. M. Jin, and J. Q. Li, *Phys. Rev. C* **80**, 067601 (2009).
- [40] G. G. Adamian, N. V. Antonenko, V. V. Sargsyan, and W. Scheid, *Phys. Rev. C* **81**, 024604 (2010).
- [41] L. Zhu, Z. Q. Feng, and F. S. Zhang, *J. Phys. G: Nucl. Part. Phys.* **42**, 085102 (2015).
- [42] M. H. Mun, G. G. Adamian, N. V. Antonenko, Y. Oh, and Y. Kim, *Phys. Rev. C* **91**, 054610 (2015).
- [43] G. G. Adamian, N. V. Antonenko, A. Diaz-Torres, and S. Heinz, *Eur. Phys. J. A* **56**, 47 (2020).
- [44] X. R. Zhang, G. Zhang, J. J. Li, S. H. Cheng, Z. Liu, and F. S. Zhang, *Phys. Rev. C* **103**, 024608 (2021).
- [45] F. Niu, P. H. Chen, Y. F. Guo, C. W. Ma, and Z. Q. Feng, *Phys. Rev. C* **97**, 034609 (2018).
- [46] A. Winther, *Nucl. Phys. A* **572**, 191 (1994).
- [47] A. Winther, *Nucl. Phys. A* **594**, 203 (1995).
- [48] R. Yanez and W. Loveland, *Phys. Rev. C* **91**, 044608 (2015).
- [49] C. Simenel, *Phys. Rev. Lett.* **106**, 112502 (2011).
- [50] S. Ayik, *Phys. Lett. B* **658**, 174 (2008).
- [51] K. Sekizawa and K. Yabana, *Phys. Rev. C* **93**, 054616 (2016).
- [52] S. Ayik, B. Yilmaz, O. Yilmaz, and A. S. Umar, *Phys. Rev. C* **100**, 014609 (2019).
- [53] V. Zagrebaev and W. Greiner, *J. Phys. G: Nucl. Part. Phys.* **31**, 825 (2005).
- [54] V. I. Zagrebaev, B. Fornal, S. Leoni, and W. Greiner, *Phys. Rev. C* **89**, 054608 (2014).
- [55] B. J. Cai and B. A. Li, *Phys. Rev. C* **93**, 014619 (2016).
- [56] N. Wang and L. Guo, *Phys. Lett. B* **760**, 236 (2016).
- [57] K. Zhao, Z. Li, N. Wang, Y. Zhang, Q. Li, Y. Wang, and X. Wu, *Phys. Rev. C* **92**, 024613 (2015).
- [58] J. Tian, X. Wu, K. Zhao, Y. Zhang, and Z. Li, *Phys. Rev. C* **77**, 064603 (2008).
- [59] L. Zhu, *Chin. Phys. C* **43**, 124103 (2019).
- [60] M. H. Mun, K. Kwak, G. G. Adamian, and N. V. Antonenko, *Phys. Rev. C* **99**, 054627 (2019).
- [61] P. W. Wen, C. Li, L. Zhu, C. j. Lin, and F.-s. Zhang, *J. Phys. G: Nucl. Part. Phys.* **44**, 115101 (2017).
- [62] R. B. Welch, K. J. Moody, K. E. Gregorich, D. Lee, and G. T. Seaborg, *Phys. Rev. C* **35**, 204 (1987).
- [63] S. Ayik, B. Schürmann, and W. Nörenberg, *Z. Phys. A* **277**, 299 (1976).
- [64] J. Q. Li, X. T. Tang, and G. Wolschin, *Phys. Lett. B* **105**, 107 (1981).
- [65] G. Adamian, N. Antonenko, and W. Scheid, *Nucl. Phys. A* **618**, 176 (1997).
- [66] G. Adamian, N. Antonenko, W. Scheid, and V. Volkov, *Nucl. Phys. A* **633**, 409 (1998).
- [67] P. Möller, J. Nix, W. Myers, and W. Swiatecki, *At. Data Nucl. Data Tables* **59**, 185 (1995).
- [68] G. Pollarolo, *Phys. Rev. Lett.* **100**, 252701 (2008).
- [69] P. W. Wen, C. J. Lin, C. Li, L. Zhu, F. Zhang, F. S. Zhang, H. M. Jia, F. Yang, N. R. Ma, L. J. Sun, D. X. Wang, F. P. Zhong, H. H. Sun, L. Yang, and X. X. Xu, *Phys. Rev. C* **99**, 034606 (2019).
- [70] K. Dietrich and K. Hara, *Nucl. Phys. A* **211**, 349 (1973).
- [71] G. Pollarolo and A. Winther, *Phys. Rev. C* **62**, 054611 (2000).
- [72] S. Szilner, L. Corradi, G. Pollarolo, S. Beghini, R. B. Behera, E. Fioretto, A. Gadea, F. Haas, A. Latina, G. Montagnoli, F. Scarlassara, A. M. Stefanini, M. Trotta, A. M. Vinodkumar, and Y. Wu, *Phys. Rev. C* **71**, 044610 (2005).
- [73] F. L. H. Wolfs, *Phys. Rev. C* **36**, 1379 (1987).
- [74] R. Bass, *Phys. Rev. Lett.* **39**, 265 (1977).
- [75] A. Ghiorso, S. G. Thompson, G. H. Higgins, B. G. Harvey, and G. T. Seaborg, *Phys. Rev.* **95**, 293 (1954).